# Bismuth Self-Limiting Growth of ultra-thin $BiFeO_3$ Films

Nitin Deepak[†,‡,*], Patrick Carolan[†], Lynette Keeney[†], Panfeng F. Zhang[†], Martyn E. Pemble[†,‡] and Roger W. Whatmore[†,‡,§,*]

[†]Tyndall National Institute, University College Cork, 'Lee Maltings', Dyke Parade, Cork, Ireland

[‡]Department of Chemistry, University College Cork, Dyke Parade, Cork, Ireland

[§]Department of Materials, Faculty of Engineering, Imperial College London, London, SW7 2AZ, UK

*KEYWORDS Ferroelectrics, self-limiting, thin films, growth, chemical vapour deposition.*

**ABSTRACT:** Bismuth ferrite ($BiFeO_3$) is a widely studied material due to its interesting multiferroic properties. Bismuth self-limiting growth pure, single-phase of $BiFeO_3$ (BFO) has previously been achieved using molecular beam epitaxy (MBE), but the growth of BFO by chemical vapour deposition (CVD) has proved to be very challenging, due to the volatile nature of bismuth. The growth window regarding temperature, pressure and precursor flow rates that will give a pure perovskite BFO phase is normally very small. In this work we have studied the metal-organic CVD (MOCVD) growth of epitaxial BFO thin films on $SrTiO_3$ substrates and found that by carefully controlling the amount of the iron precursor, $Fe(thd)_3$, where thd = 2,2,6,6 tetra methyl 3,5 heptanedionate, we were able to achieve bismuth self-liming growth, for the first time. The effect of the volume of the bismuth and iron precursors injected on the growth of BFO thin films is reported and it has been found that the phase-pure films can be prepared when the Bi/Fe ratios are between 1.33 and 1.81 at temperature and pressure conditions of 650°C and 10 mbar respectively and where the $O_2$ gas flow was kept constant to 1000sccm out of 3000sccm total gas flow. Piezoresponse force microscopy (PFM) studies demonstrate the presence of bipolar- switching in ultra-thin BFO films.

## INTRODUCTION

Multiferroic materials[1], which exhibit the simultaneous existence of ferroelectric and ferromagnetic properties, have been studied in the recent past because of their potential for various future electronic device applications such as magnetoelectric random access memories (MERAM)[2], spin-valves[3], and multiferroic tunnel junctions[4, 5]. Bismuth ferrite - $BiFeO_3$[6] (BFO) is one of the few materials showing multiferroic properties at room temperature. The high Néel and ferroelectric Curie temperatures[7] of BFO (370°C and 827°C respectively) also make it a good candidate for various high temperature applications, such as high temperature piezoelectric devices[8]. BFO possesses a perovskite unit cell with a ferroelectric rhombohedral structure[9] at room-temperature with point group *R3c*, a lattice parameter of 3.965Å and rhombohedral angle of 89.3–89.48°. The ferroelectric polarization direction is along the $[111]_{pseudocubic}$ axis. BFO thin films were previously grown with various high vacuum methods, such as molecular beam epitaxy (MBE)[10] and pulsed laser deposition (PLD)[6]. These methods give very good control over thin film growth, but there is a tendency for the formation of oxygen vacancies due to incomplete metallic oxidation which often leads to n-type conductivity, which gives electrical leakage problems[11].

BFO thin films have been grown previously with metal-organic chemical vapour deposition (MOCVD) methods,[12-14] as these methods can coat larger areas more quickly and with fewer oxygen vacancies as compared with high vacuum techniques. Furthermore, excellent control over the domain structure of CVD-grown BFO films was shown by Yang *et al.*[15]. In this report, BFO films were prepared with purely 71° and 109° surface domains by carefully straining films by growth on $DyScO_3$ substrates using the liquid injection MOCVD method[15].

In MOCVD, film growth temperature, pressure, and gas flows in the reaction chambers all play an important role during the deposition. Usually, high temperatures are required for complete pyrolysis of precursors, as compared to MBE growth where metallic vapours are used. Another important parameter that drives the stoichiometry during MOCVD film growth is the precursor injection rates which can be used to ensure accurate compositional control. In the case of BFO films, this essential parameter is also defined as the relative Bi and Fe precursor injection ratio. The range of relative Bi to Fe precursor ratio, in which phase-pure BFO films can be prepared, is called the growth window. This growth window for pure BFO films as reported in literature[12, 13] is small, and it requires strict control for stoichiometric growth. For stoichiometric BFO thin films using the same type of precursors, Thery *et al.*[13] reported a Bi/Fe precursor injection ratio of 2.5, whereas Yang *et al.*[12] reported a ratio of 2.33. The slight difference between these two values can be attributed to different growth conditions, such as substrate temperature and reactor pressure. The use of higher bismuth injection volumes as compared to iron precursor is to compensate for the bismuth deficiency due to the volatile nature of bismuth. Deviation from the growth win-

dow often leads to the presence of impurity phases, such as iron or bismuth oxides. The presence of iron oxide can cause a spurious ferromagnetic signal which can be of two orders higher than pure BFO films[16] whereas bismuth oxide impurities can lead to leakage currents which degrade the film's electrical properties[16].

The volatile nature of elemental bismuth or bismuth oxide can be exploited to prepare phase-pure BFO films by using a bismuth self-limiting process, in which a significantly higher amount of volatile component (Bi) of films and the right amount of non-volatile components (Fe) are provided but stoichiometry still can be achieved. There are various examples in literature exploiting this self-limiting process for the growth of technologically important compounds such as $PbTiO_3$[17] and GaAs[18-21] with MBE. The vaporization of PbO and As from the film surface limits the Pb and As content in $PbTiO_3$ and GaAs thin films respectively. Similar bismuth self-limiting growth processes were used for the growth of BFO thin films with MBE[10], where Ihlefeld *et al.*[10] suggested that the growth of pure BFO films can be achieved with temperature and Bi/Fe flux ratios ranging from 4/1 to 8/1 for 330 to 420ºC and respectively.

Self-limiting film growth is rare for oxide MOCVD processes. $PbTiO_3$ thin films growth is one example[22, 23]. There are no self-limiting growth processes reported in the literature for BFO thin films. The advantage of self-limiting MOCVD growth is the extension of the growth window for BFO thin films by MOCVD processes. The use of higher bismuth precursor flow leads to the absence of iron oxide in BFO thin films and hence no false magnetic signal. In this paper we report the first observation of bismuth self-limiting growth of epitaxial BFO thin films with MOCVD on $SrTiO_3$ (STO) substrates. This MOCVD self-limiting process is different from atomic layer deposition (ALD) method. With ALD method self-limiting behavior can be achieved for both Bi and Fe precursors due to the surface reactions limited by kinetics[24]. The films prepared by ALD are usually amorphous and need post-deposition annealing.

## EXPERIMENTAL SECTION

### THIN FILM DEPOSITION

BFO thin films were prepared with an AIXTRON AIX 200/4FE AVD[25] (atomic vapour deposition, or liquid injection MOCVD) system. $Bi(thd)_3$ and $Fe(thd)_3$ (where thd = 2,2,6,6-tetramethyl 3,5-heptanedionate) were dissolved in toluene and used as bismuth and iron precursor solutions respectively. The final concentration of the precursor solutions was 0.1M. Precursor solutions were carried from stainless steel storage bottles to a vaporizer with the help of nitrogen gas. The precursors were injected into a vaporizer kept at 220ºC. The injected precursor volume was controlled by adjusting the numbers of pulses and the opening time of injector for each pulse. The bismuth and iron precursors were injected alternately as $(Bi\text{-}5s\text{-}Fe\text{-}5s)_n$, where 'n' is the number of times this precursor sequence was repeated to get the desired thickness. The precursor injection sequence is shown in figure S1 (supplementary information). This is called the "alternating injection mode" to distinguish it from the more-conventional continuous injection mode[25, 26]. Table S1 (supplementary information) show how the precursor flow was changed during each film growth and its effect on growth rate.

The value of n is kept constant to 20 and the time between each set of pulses is set at 5s for the first two cases discussed below, but is varied for the third study. Each bismuth or iron precursor pulse set consists of individual pulses with a given injector opening time (see figure S1). The frequency of the individual pulses was 1 Hz. The vapours formed inside the vaporizer were then carried towards the film growth reactor (chamber) using $N_2$ through heated lines kept at a temperature of 220ºC. The substrate was kept on a heated graphite susceptor with an embedded thermocouple to measure the temperature. The temperature of the substrate was maintained at 650ºC. Pure $O_2$ was used as an oxidizing agent. The total gas flow in the reactor was kept constant to 3000sccm. The $O_2$ gas flow is kept to 1000sccm. All the films were grown on single crystalline (001) oriented $SrTiO_3$ (STO) substrates. Niobium doped STO (0.7 weight %) substrates were used for BFO films growth for the piezoresponse force microscopy (PFM) analysis. The substrates were cleaned with acetone and isopropanol prior to deposition. The $O_2$ supply was switched off after precursor injection and cooling of the films was performed under the inert $N_2$ gas environment.

### THIN FILM CHARACTERIZATION

All thin film samples were analyzed at room temperature. The crystal structure of BFO thin films was analyzed by Phillips Panalytical MRD x-ray diffraction (XRD) system with conditioned Cu k-$\alpha$ radiation with Göebel mirror setup. Thickness analysis was performed with low angle x-ray reflectivity (XRR) measurements and X'pert reflectivity software. X-ray photoelectron spectroscopy (XPS) experiments were conducted on a Thermo K-alpha machine with an Al $K_\alpha$ x-ray source. All binding energies were referenced to C1s peak at 285 eV. High resolution transmission electron microscopy (HRTEM) imaging was performed using JEOL 2100 TEM with a $LaB_6$ source operated at 200kV. Sample preparation for TEM analysis was done using an FEI Quanta 3D 200i dual beam focused ion beam (FIB) system. Topographic height images were obtained using a MFP-3D™ (Asylum research) atomic force microscope (AFM) in semi-contact mode. Piezoresponse force microscopy (PFM) was used in dual AC resonance tracking (DART)[27] contact-mode. Platinum coated silicon tips with contact resonance frequency around 300 kHz were used for PFM measurements. PFM switching spectroscopy was used to obtain the hysteresis and amplitude loops to analyze the local switching behavior of the BFO thin films.

## RESULTS AND DISCUSSION

Three different sets of experiments were performed to understand the growth of BFO thin films. In the first set of experiments, thin films were prepared by keeping the bismuth precursor flow constant and varying the iron precursor flow. Figure 1 shows the XRD plot of BFO thin films, prepared with the first set of experimental conditions. All graphs were plotted according to the injected volumetric Bi/Fe ratios used during film deposition with the intensity in logarithmic scale to emphasize weak peaks and with an offset between each graph for better comparison. All the substrate and sample holder peaks are labeled with asterisk '*' sign. The amount of bismuth is kept higher than the required stoichiometric ratio. The Bi/Fe ratio was changed from 3.32 to 1.94. All the BFO thin films are highly *c*-axis oriented, as can be observed from the XRD plots shown in figure 1. Films with Bi/Fe ratios from

3.32 to 2.30 show weak impurity peaks around 2Theta values of 31.75° and 32.50°.

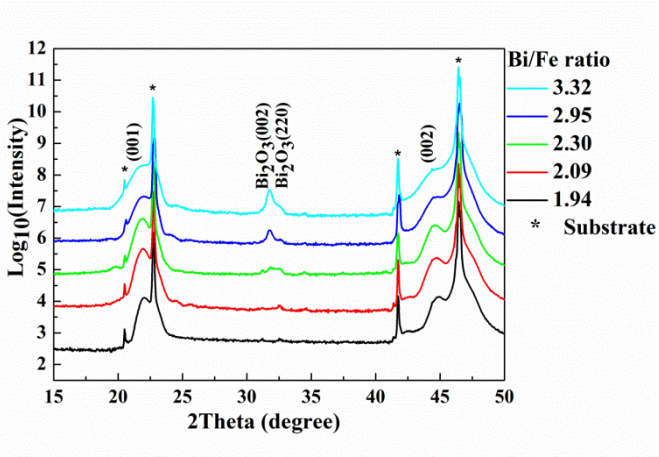


**Figure 1** XRD plots for thin films on STO substrates prepared by keeping the bismuth precursor flow constant and varying the iron precursor flow. Peaks labelled with '*' were from substrate or sample holder.

The intensities of the impurity peaks decrease with a decrease in Bi/Fe ratio. The data analysis shows the presence of bismuth oxide ($Bi_2O_3$) as an impurity phase[28]. The $Bi_2O_3$ phase occurs due to high bismuth precursor flow as compared to Fe precursor flow. With a further increase in the iron precursor flow, decreasing the Bi/Fe ratio to 2.09, the $Bi_2O_3$ (002) and (220) peaks disappear and a pure BFO phase can be observed. The XRD data shows no sign of $Bi_2O_3$ impurity within the detection limit of the instrument. Figure 2 shows the relative change in $Bi_2O_3$ impurity content with change in Bi/Fe ratio from 3.32 to 1.94.

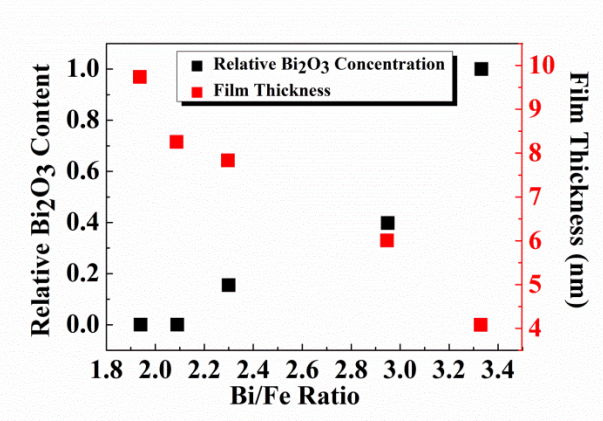


**Figure 2** The relative variation of $Bi_2O_3$ content and thickness plotted against Bi/Fe ratio.

The variation of film thickness (as measured with XRR plots shown in figure S2) with Bi/Fe ratio was plotted and is shown in figure 2. An interesting trend was observed where the film thickness, and hence the growth rate, increases on increasing the iron precursor flow. Interestingly, at a Bi/Fe ratio of 2.09, the measured thickness of the film is 8.2 nm and the growth rate per AVD cycle [$(Bi\text{-}5s\text{-}Fe\text{-}5s)_n$, where n = 20] is 0.41 nm. The thickness of one unit cell of BFO in the 'c' direction is 0.3965nm which is very close to growth rate per cycle at this Bi/Fe ratio. Thus, the phase-pure BFO thin films are formed when the growth rate per cycle reaches a value near to, or higher than, that required to deposit a monolayer of BFO. This situation is similar to the growth of BFO films by MBE[10], where the quantities of metallic iron vapours are usually controlled to insert a monolayer of BFO.

Laboratory XRD systems are relatively insensitive to the presence of second-phase impurities at low levels, with a limit of detection of around 2 vol%[29]. Thus, there is a possibility of impurities even if none can be seen by standard XRD methods. It is thus important to analyze for the presence of low-level impurities with other analytical techniques. In the case of BFO films, AFM can help in analyzing the presence of second phase impurities, as films with these show a distinct surface topography[12-14, 16, 30] (such square features). Figure S3 (supplementary information) shows the variation of film topography and RMS roughness with the variation in Bi/Fe ratio for the first set of experiments. The film surface became smoother with the increase in iron injection. Starting with the Bi/Fe ratio of 3.32 (figure S3a) the film is rough with the RMS roughness values of 10.50 nm and the roughness decreases to 1.49 nm (figure S3e) when the ratio reaches to 1.94. This decrease in roughness of the film surface is due to a decrease in the amount of impurities present on the film's surface (figure 2). The surface has round features and the population of these features decreases with increase in iron content. There is a slight increase in roughness from Bi/Fe ratio 3.32 (10.50 nm) to Bi/Fe ratio 2.30 (12.75 nm). The films with low impurity content (Bi/Fe ratio 2.30) can have an uneven spread of impurities on the films surface as compared to films with high impurity content (Bi/Fe ratio of 3.32), which give rise to slightly higher surface roughness. There is a dramatic reduction in surface roughness in going from a Bi/Fe ratio of 2.3 to 2.09. Nevertheless, the AFM images for the lowest Bi/Fe ratio of 1.94 (figure S3e) still show some round surface features which point toward the presence of bismuth oxide impurities. The films at this Bi/Fe ratio were not atomically smooth (roughness > 1 nm). $Bi_2O_3$ impurities usually occur with square or rectangular facets. To rule out any possibility of AFM tip distortion artifacts[31], scanning electron microscopy was performed on these samples.

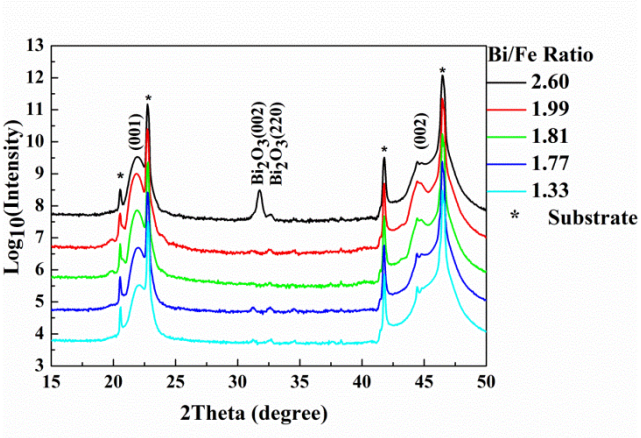


**Figure 3** XRD plots demonstrating the growth of BFO thin films on STO substrates by keeping the iron precursor flow constant and varying the bismuth precursor flow at 650ºC.

Figure S4 shows SEM surface images for the first set of experiments. Clear square patterns were observed which again confirms the presence of $Bi_2O_3$ impurities. The population of these $Bi_2O_3$ impurities is decreasing with increase in iron flow.

Bismuth volatility is one of the major problems in reproducing phase-pure bismuth containing oxide thin films. There is a formation of bismuth oxide impurities with excess bismuth flow and iron oxide impurities at low bismuth flows as discussed before. In order to evaluate the effects of bismuth precursor flow, and to improve the surface roughness, a second set of experiments was performed, where the iron precursor flow was kept constant and the bismuth precursor flow was varied. The iron precursor flow was selected below the range in the first set of experiments where the pure BFO phase occurs (Bi/Fe ratio 1.77). Figure 3 shows the effect of the variation of the bismuth precursor flow on the crystalline nature of BFO thin films. The bismuth precursor flow was firstly decreased to change the Bi/Fe ratio from 1.77 to 1.33. Phase-pure BFO phase occurs at a Bi/Fe ratio of as low as 1.33. At the other end of the second set of experiments, an increase in bismuth precursor flow (from Bi/Fe ratio 1.77 to 1.99) also produced phase-pure films. A further increase in bismuth flow (Bi/Fe ratio 2.60) causes the formation of the $Bi_2O_3$ impurity phase. This set of experiments gives an upper bound on the bismuth precursor injection flow. These results are the same as conventional MOCVD growth mode, where a higher bismuth flow causes the formation of a $Bi_2O_3$ impurity. For the second set of experiments, figure S5 (supplementary information) shows the change in film topography and RMS roughness with Bi/Fe ratio. The film roughness decreases drastically from the values of 6.55 nm to 0.22 nm with the change of Bi/Fe ratio from 2.60 to 1.33 respectively. At a Bi/Fe ratio of 2.60, square faceted surface features can be observed and below this Bi/Fe ratios the surface of the films becomes atomically smooth. The reason for high surface roughness is usually due to the presence of bismuth oxide impurities[12, 16]. As the Bi/Fe ratio approaches 1.81 down to 1.33 the film surface become atomically smooth with RMS roughness below 0.4 nm. Thickness analysis was performed for this set of experiment with XRR (plots are shown in figure S5) and the variation of film thickness with Bi/Fe ratio is shown in figure 4. It can be observed that the film thickness remain nearly constant around 10 nm for varying bismuth flows. This observation points towards the independence of growth rate on bismuth precursor flow. The excess bismuth stays on the film surface in the form of $Bi_2O_3$ impurities, but in the region, where Bi/Fe ratio is between 1.33 to 1.81, the bismuth self-limiting process appears and phase pure BFO films are formed.

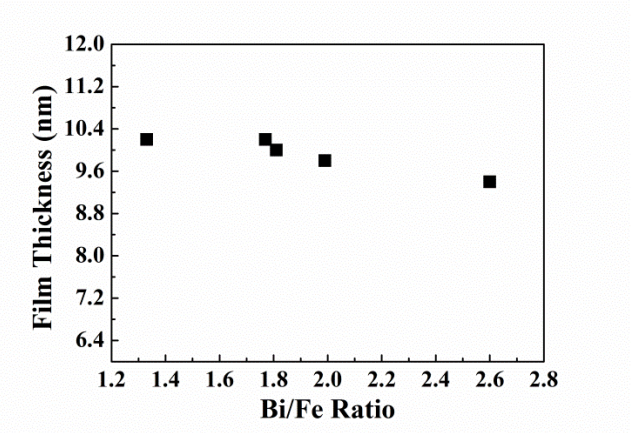


**Figure 4** The variation of thickness plotted against Bi/Fe ratio for BFO films grown at constant Fe precursor flow.

Figure S7 (supplementary information) shows the SEM surface images for second set of experiments. Similar trend as that of AFM imaging was observed. In-plane phi scans were performed on the sample with Bi/Fe ratio of 1.81. Figure S6 (supplementary information) shows the phi scan on the (101) BFO peak and the (202) STO peak. The presence of four distinct peaks were observed at an interval of 90° confirms the epitaxial nature of BFO thin film grown on STO substrates.

In CVD processes, the residence time of precursor vapours inside the reaction chamber affects the growth of films. In case of bismuth-containing films larger or smaller residence times may lead to the formation of impurities. The residence time of precursor vapours can be varied in many ways such as changing the gas flow rates or pressure inside the reaction chamber[14]. In the present case, the time difference between each set of pulses is changed from 5s to 15s to assess the evolution of the structure of the BFO thin films. The increase in time between pulses increases the purging time before the arrival of the next precursor pulse. This increase in time decreases the residence time of the vapours in the chamber which is likely to result in an increase in the extent of desorption of elemental bismuth or bismuth oxide from the surface of the substrate. The Bi/Fe precursor ratio was kept constant at the value of 2.60 used from the second set of experiments where $Bi_2O_3$ impurities were present. Figure 5 shows the effect of time between various set of pulses by keeping the bismuth and iron precursor flow constant. The BFO films prepared showed the $Bi_2O_3$ impurity phase when the time difference between each set of pulses was 5s. On increasing the time difference to 10s there is a decrease in the intensity of the $Bi_2O_3$ peaks.

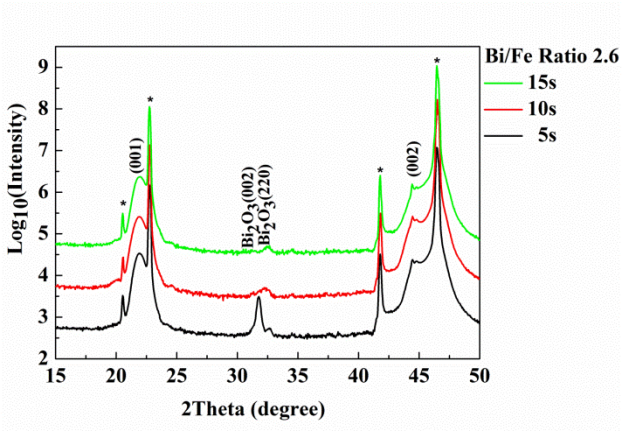


**Figure 5** XRD plots for the growth of thin films by keeping the iron and bismuth precursor flow constant and varying the time difference between each set of pulses.

On further increasing the time difference to 15s, the formation of the pure BFO phase occurs. This change from an impure to a pure BFO phase simply by changing the time difference in the presence of the same quantity of bismuth and iron flow strongly indicates the presence of bismuth desorption processes leading to self-limiting growth.

AFM analysis was performed at various times between each pulse set. Figure S7 (supplementary information) shows the variation of film topography and RMS roughness with the change in time between each set of pulses at constant iron and bismuth precursor flows. The films tend to get smoother, but there is still the presence of square faceted structures on the film surface, even when XRD shows the absence of bismuth oxide impurities at time difference of 15s. Interestingly, the size of these bismuth oxide impurities decreases slightly with increasing the time difference. This can be due to desorption of bismuth from the surface resulting in smaller bismuth oxide crystals on the surface. This observation concluded that even though there is an absence of impurities shown by XRD there are still lots of structural features present on the films' surfaces which may not be crystalline in nature.

The presence of Fe sites in 2+ oxidation state could affect the magnetic properties of the BFO films. In order to assess this possibility, XPS analysis was performed. Two different samples from the second set of experiments with Bi/Fe ratio of 1.77 and 1.33 were used. XPS spectra were acquired both on the as-deposited samples and after cleaning with an $Ar^+$ ion beam to improve the signal-to-noise ratio. Figure S8 (supplementary information) show wide range XPS survey spectra, core-level Fe 2p spectra and core-level C1s scan for films grown at Bi/Fe ratio 1.77, both before and after the cleaning with $Ar^+$ for three minutes. All data was calibrated with the C1s peak present at 285 eV. The Fe2p core level spectrum in figure S8b shows a clear Fe 2p3/2 peak at 711.04 eV and a Fe 2p1/2 peak at 724.05 eV. This observation confirms the presence of $Fe^{3+}$ in the BFO thin film grown at Bi/Fe ratio 1.77. Figure S9 (supplementary information) shows the wide range XPS survey spectra, core-level Fe2p spectra and a core-level C1s scan for films grown at lowest Bi/Fe ratio of 1.33, before and after $Ar^+$ ion cleaning. Fe2p core level spectra show a considerable difference between 2p1/2 and 2p3/2 peak position before and after the cleaning step. This BFO sample before cleaning shows only the presence of $Fe^{3+}$, but the position of Fe 2p3/2 peak shifts from 711.15 eV to 709.5 eV and Fe 2p1/2 shifts from 724.9 eV to 722.56 eV after cleaning. This shift can be attributed to the removal of oxygen from the BFO lattice by the $Ar^+$ ion cleaning step, thus reducing the Fe to form $Fe^{2+}$. It is interesting to note that the film with Bi/Fe ratio 1.77 showed a significantly larger improvement in S/N ratio after cleaning relative to the film with Bi/Fe ratio 1.33. This may be because the films prepared with slightly higher Bi content have a very thin layer of excess Bi or presence of more environmental carbon, on the surface prior to cleaning which is preventing the Fe electrons from reaching the detector. Such a layer would only need to be a few atomic layers thick to have an effect on photoelectron electron emission. For the film with Bi/Fe ratio 1.33, the absence of such a layer on the surface means that the iron in the film is more-readily reduced to $Fe^{2+}$ during $Ar^+$ ion cleaning relative to the film grown with Bi/Fe ratio of 1.77.

There are, thus, three factors that enable self-limiting BFO film growth. The first factor is the particular injection mode used during film growth. The alternating injection growth mode works differently from the conventional continuous injection mode. The injection of precursors in alternating pulses is the key factor which helps in efficient decomposition of precursor, which leads to the deposition at much lower Bi/Fe ratios[12, 32] (as low as 1.33). In one of our previous report of AVD growth of $Bi_5FeTi_3O_{15}$ by the pulsed precursor injection mode only 8% bismuth excess was required to compensate for the bismuth volatility,[32] which demonstrates the efficiency of this growth mode. The second factor that is responsible for the self-limiting growth is the control over iron precursor flow. Once the iron precursor injection volume becomes more than that required to insert one monolayer of BFO, the bismuth oxide impurity content decreases drastically. This behavior is similar to some of the thin film systems studied by MBE ($PbTiO_3$ and $Bi_4Ti_3O_{12}$) where a control over titanium flux was required[33]. The third factor is to keep the bismuth precursor flow in a certain range once the iron precursor flow is more than that required to insert one monolayer of BFO. Demonstration of a constant BFO film thickness on variation of Bi flows (with fixed iron precursor flow) shows that the growth rate is independent of the bismuth precursor flow. The presence of bismuth oxide impurities on the film surface was still evident. The time difference between pulse sets decreases the bismuth oxide impurity content but control over the bismuth precursor flow is still required. This process does not show the self-limiting growth for the whole range of bismuth precursor flow as compared to MBE growth but it still extends the growth window as compared to previous reports[12, 13].

## TEM CHARACTERIZATION

TEM characterization was performed to analyze the local crystalline structure of the BFO thin film. Figure 6 shows a HRTEM image of the BFO thin film. This image demonstrates the crystalline nature of the BFO films with a sharp interface between film and substrate, confirming the absence of interfacial defects. The inset image shows the fast Fourier transform (FFT) of the TEM image shown in figure 6. The FFT image shows high ordering of the atomic planes in the films and pseudo-cubic structure of the BFO film.

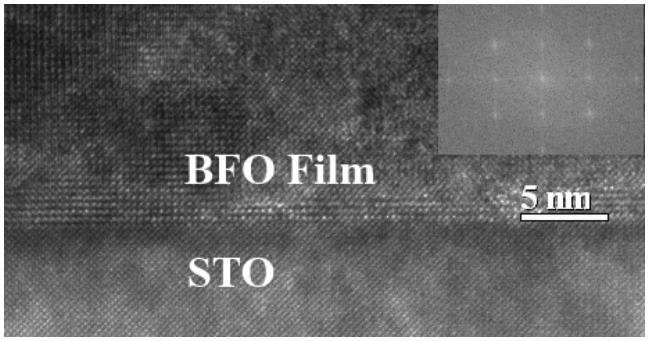


**Figure 6** A HRTEM bright filed image showing the crystalline nature of the film and a sharp interface with the substrate. The inset image shows the fast Fourier transform (FFT) of the BFO film obtained from the HRTEM image.

## PFM MEASUREMENTS

A 10nm thick BFO film prepared on Nb-STO, with Bi/Fe ratio of 1.81 at 5s time difference, was used for the PFM measurements. PFM switching spectroscopy[34] is used to understand the nanoscale switching dynamics of ferroelectric films.

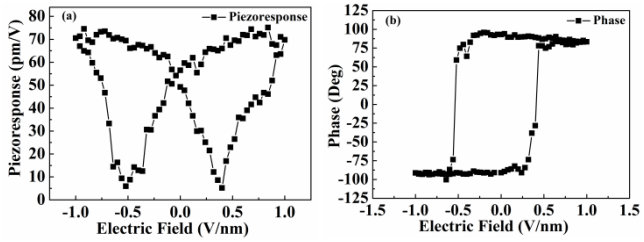


**Figure 7** The PFM **(a)** amplitude butterfly loop (piezoresponse), and **(b)** phase hysteresis loop for BFO thin film deposited on Nb doped STO. Please note that the piezoresponse is an amplified response due to DART-PFM mode used.

A nanosize tip applies a DC bias to the film surface, to locally excite the domains due to the converse-piezoelectric effect. The phase and amplitude of excitation is then measured by the deflection of the tip. The typical amplitude butterfly and 180° phase hysteresis loops obtained are signatures of ferroelectric behavior. Figure 7a and 7b shows the typical amplitude strain butterfly loop and phase loop for BFO thin films. 180° phase switching can be observed in figure 7b, which is an indication of ferroelectric switching behavior. The coercive field was calculated from the phase image in figure 7b. The calculated value is 4800kVcm$^{-1}$. Most of the coercive field values reported for BFO films are for thicker films ranging from 320 to 640 nm films[35, 36]. $E_C$ (coercive field) values were extrapolated from previous reports[35, 36] using the Kay-Dunn scaling law $E_C \alpha t^{-2/3}$ , where t is film thickness[37]. (The literature data fit to this scaling law well, with an exponent of -0.66.) The value of $E_C$ for a 10nm film as calculated by extrapolation from this data, as shown in the plot in figure S10, was 1209 kVcm$^{-1}$. This value is approximately 4 times smaller than the value measured in this work. It is possible that the values measured here may be affected by the effective film thickness being thinner than the nominal value of 10nm. The presence of a dead-layer at film-substrate interface, the presence of interfacial charges etc. could be responsible for this. Such layers can not only affect the properties of ultra-thin ferroelectric films but can completely suppress the polarization[38, 39]. A further interpretation of the increased coercive field could come by applying a depolarization correction. Dawber et al.[40] have applied depolarization corrections to the above scaling law and have shown that for certain electrode types, very significant increases in coercive field relative to the Kay-Dunn scaling law can be expected, depending on the electrode type. Further studies would be required to fully explain which phenomenon is effective in this case.

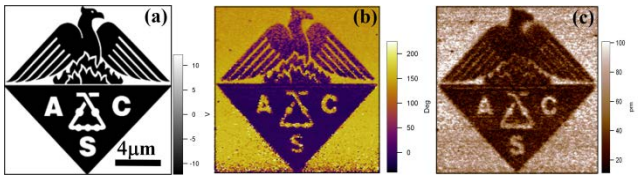


**Figure 8** The **(a)** American chemical society logo that is written as domains on the surface of BFO thin film with voltages ±15V. The figure shows PFM **(b)** amplitude and **(c)** phase images after the write step. (The logo used was downloaded from http://www.acs.org/content/acs/en.html.)

Piezoelectric coefficient $d_{33}$ was calculated from PFM amplitude images. Two steps were used for PFM calibration[41] in DART mode. A piece of silicon was used to calculate the PFM background noise and α-quartz ($d_{33}$ =-2.3pm/V) was used for calibrating PFM signal. PFM amplitude images shown in figure S13 (supplementary information) for silicon, α-quartz, and BFO thin film, were used to calculate $d_{33}$. The calculated value of $d_{33}$ is 8.48pm/V. This calculated value is in close agreement with previously reported values by Zhao *et al*[42]. Ferroelectric materials were studied for their polarization retention properties on application of an electric field higher than the film's coercive fields. PFM is an excellent tool to study the polarization behavior of materials at the nanoscale. PFM can write +ve or –ve domains on the surface of a ferroelectric by application of bias to a conducting tip. The same conducting tip can read the written polarization state in a second step. A bitmap image of the American Chemical Society (ACS) logo, as shown in figure 8a, was written on the BFO film surface with the application of ±15V DC bias to the PFM tip. The PFM imaging was performed with 2.5V AC bias after the writing step. The amplitude contrast can be observed in figure 8b between those two regions poled with +ve and –ve voltages. Figure 8c shows the PFM phase image after poling. The clear 180° phase switching can be observed between two regions poled with +ve and –ve regions as shown in figure 8a. This retention of polarization by the BFO thin film after poling proves its ferroelectric nature. The fact that polarization states can be "written" and retained on removal of an applied electric field makes these materials excellent candidates for non-volatile random access memory applications[43]. The data written in the form of the ACS logo on the BFO film surface shows the versatility of PFM to pole the film surface regions in different shapes.

## CONCLUSION

Ultra-thin BFO films were successfully prepared by liquid injection MOVCD (AVD) method in a layer-by-layer growth mode onto a (001) STO substrates. All films show single crystalline orientation. Sub-monolayer precision was demonstrated for the BFO film deposition. It has been found that the insertion of a monolayer of BFO as a consequence of controlling the iron precursor flow plays an important role in achieving

bismuth self-limiting growth. This is the first observation of growth of BFO thin films by bismuth self-limiting behavior in a CVD process. The growth window for bismuth precursor flow was identified where self-limiting growth was achieved. The Bi/Fe ratios of 1.33 to 1.81 were used to grow phase-pure BFO at growth temperature of 650°C and pressure of 10 mbar. The total $O_2$ flow in the reaction chamber was 1000sccm (out of 300sccm total flow). This process can be extended to other bismuth containing oxides. This process can help in achieving phase-pure bismuth containing oxide films over a wide range of precursor injection ratios and hence eliminating the need to control some parameters tightly (like bismuth injection volumes) during the CVD growth and may open-up up a way to prepare BFO thin films for industrial scale deposition. PFM measurement confirmed the presence of ferroelectric switching behavior in ultra-thin BFO films. Ferroelectric polarization states were written on the BFO thin film surface. The poling behavior confirmed the retention of polarization states of BFO thin films, demonstrating that these films could be used for non-volatile memory applications.

## ASSOCIATED CONTENT

**Supporting Information**

The film growth sequence and AFM images at various growth conditions. "This material is available free of charge via the Internet at http://pubs.acs.org."

## AUTHOR INFORMATION

### Corresponding Author

*** Nitin Deepak and Roger W. Whatmore[§]**

Email: nitin.deepak@tyndall.ie, roger.whatmore@tyndall.ie

### Present Addresses

§ Department of Materials, Faculty of Engineering, Imperial College London, London, SW7 2AZ, UK

### Author Contributions

The manuscript was written through contributions of all authors.

### Funding Sources

The authors acknowledge ICGEE (International Centre for Graduate Education in Micro & Nano Engineering) for funding N. D. PhD. The support of Science Foundation Ireland (SFI) under the FORME Strategic Research Cluster Award number 07/SRC/I1172 is greatly acknowledged. This research was also enabled by the Higher Education Authority Program for Research in Third Level Institutions (2007-2011) via the INSPIRE program.

## ACKNOWLEDGMENT

Authors would like to thanks Vince Lodge for the help in preparing TEM sample with FIB. Authors would like to acknowledge Pete Fleming for his help in performing XPS experiments.

## ABBREVIATIONS

CVD, Chemical Vapour Deposition; PFM, Piezoresponse force microscopy;

## REFERENCES

1. Fiebig, M., Revival of the magnetoelectric effect. *Journal of Physics D-Applied Physics* **2005,** 38, (8), R123-R152.

2. Bibes, M.; Barthelemy, A., Multiferroics: Towards a magnetoelectric memory. *Nat Mater* **2008,** 7, (6), 425-426.

3. Kleemann, W.; Binek, C., Multiferroic and Magnetoelectric Materials. In *Magnetic Nanostructures*, Zabel, H.; Farle, M., Eds. Springer Berlin Heidelberg: 2013; Vol. 246, pp 163-187.

4. Pantel, D.; Goetze, S.; Hesse, D.; Alexe, M., Reversible electrical switching of spin polarization in multiferroic tunnel junctions. *Nat Mater* **2012,** 11, (4), 289-293.

5. Tsymbal, E. Y.; Gruverman, A.; Garcia, V.; Bibes, M.; Barthélémy, A., Ferroelectric and multiferroic tunnel junctions. *MRS Bulletin* **2012,** 37, (02), 138-143.

6. Wang, J.; Neaton, J. B.; Zheng, H.; Nagarajan, V.; Ogale, S. B.; Liu, B.; Viehland, D.; Vaithyanathan, V.; Schlom, D. G.; Waghmare, U. V.; Spaldin, N. A.; Rabe, K. M.; Wuttig, M.; Ramesh, R., Epitaxial $BiFeO_3$ Multiferroic Thin Film Heterostructures. *Science* **2003,** 299, (5613), 1719-1722.

7. Spaldin, N. A.; Cheong, S.-W.; Ramesh, R., Multiferroics: Past, present, and future. *Physics Today* **2010,** 63, (10), 38-43.

8. Bennett, J.; Bell, A. J.; Stevenson, T. J.; Comyn, T. P., Tailoring the structure and piezoelectric properties of $BiFeO_3$-$(K_{0.5}Bi_{0.5})TiO_3$–$PbTiO_3$ ceramics for high temperature applications. *Applied Physics Letters* **2013,** 103, (15), -.

9. Catalan, G.; Scott, J. F., Physics and Applications of Bismuth Ferrite. *Advanced Materials* **2009,** 21, (24), 2463-2485.

10. Ihlefeld, J. F.; Kumar, A.; Gopalan, V.; Schlom, D. G.; Chen, Y. B.; Pan, X. Q.; Heeg, T.; Schubert, J.; Ke, X.; Schiffer, P.; Orenstein, J.; Martin, L. W.; Chu, Y. H.; Ramesh, R., Adsorption-controlled molecular-beam epitaxial growth of $BiFeO_3$. *Applied Physics Letters* **2007,** 91, (7), 071922-3.

11. Chambers, S. A., Molecular beam epitaxial growth of doped oxide semiconductors. *Journal of Physics: Condensed Matter* **2008,** 20, (26), 264004.

12. Yang, S. Y.; Zavaliche, F.; Mohaddes-Ardabili, L.; Vaithyanathan, V.; Schlom, D. G.; Lee, Y. J.; Chu, Y. H.; Cruz, M. P.; Zhan, Q.; Zhao, T.; Ramesh, R., Metalorganic chemical vapor deposition of lead-free ferroelectric $BiFeO_3$ films for memory applications. *Appl. Phys. Lett.* **2005,** 87, 102903.

13. Thery, J.; Dubourdieu, C.; Baron, T.; Ternon, C.; Roussel, H.; Pierre, F., MOCVD of $BiFeO_3$ Thin Films on $SrTiO_3$. *Chemical Vapor Deposition* **2007,** 13, (5), 232-238.

14. Kartavtseva, M. S.; Gorbenko, O. Y.; Kaul, A. R.; Murzina, T. V.; Savinov, S. A.; Barthélémy, A., $BiFeO_3$ thin films prepared using metalorganic chemical vapor deposition. *Thin Solid Films* **2007,** 515, (16), 6416-6421.

15. Yang, S. Y.; SeidelJ; Byrnes, S. J.; ShaferP; Yang, C. H.; Rossell, M. D.; YuP; Chu, Y. H.; Scott, J. F.; Ager, J. W.; Martin, L. W.; RameshR, Above-bandgap voltages from ferroelectric photovoltaic devices. *Nat Nano* **2010,** 5, (2), 143-147.

16. Bea, H.; Bibes, M.; Barthelemy, A.; Bouzehouane, K.; Jacquet, E.; Khodan, A.; Contour, J. P.; Fusil, S.; Wyczisk, F.; Forget, A.; Lebeugle, D.; Colson, D.; Viret, M., Influence of parasitic phases on the properties of $BiFeO_3$ epitaxial thin films. *Applied Physics Letters* **2005,** 87, (7), 072508-3.

17. Theis, C. D.; Yeh, J.; Schlom, D. G.; Hawley, M. E.; Brown, G. W., Adsorption-controlled growth of $PbTiO_3$ by

reactive molecular beam epitaxy. *Thin Solid Films* **1998,** 325, (1-2), 107-114.
18. Arthur, J. J. R., Interaction of Ga and $As_2$ Molecular Beams with GaAs Surfaces. *Journal of Applied Physics* **1968,** 39, (8), 4032-4034.
19. Cho, A. Y., Epitaxy by periodic annealing. *Surface Science* **1969,** 17, (2), 494-&.
20. Cho, A. Y., Morphology of epitaxial growth of gaas by a molecular beam method - observation of surface structures. *Journal of Applied Physics* **1970,** 41, (7), 2780-&.
21. Cho, A. Y., GaAs epitaxy by a molecular beam method - observations of surface structure on (001) face. *Journal of Applied Physics* **1971,** 42, (5), 2074-&.
22. Funakubo, H.; Hioki, T.; Otsu, M.; Shinozaki, K.; Mizutani, N., Film thickness dependence of dielectric property and crystal-structure of $PbTiO_3$ film prepared on Pt-$SiO_2$-Si substrate by metal-organic chemical-vapor-deposition. *Japanese Journal of Applied Physics Part 1-Regular Papers Short Notes & Review Papers* **1993,** 32, (9B), 4175-4178.
23. Keijser, M. d.; Dormans, G. J. M., *MRS Bull.* **1996,** 21.
24. Zhang, F.; Sun, G.; Zhao, W.; Wang, L.; Zheng, L.; Liu, S.; Liu, B.; Dong, L.; Liu, X.; Yan, G.; Tian, L.; Zeng, Y., Atomic Layer Deposition of $BiFeO_3$ Thin Films Using β-Diketonates and $H_2O$. *The Journal of Physical Chemistry C* **2013,** 117, (46), 24579-24585.
25. Deepak, N.; Zhang, P. F.; Keeney, L.; Pemble, M. E.; Whatmore, R. W., Atomic vapor deposition of bismuth titanate thin films. *Journal of Applied Physics* **2013,** 113, (18), 187207-7.
26. Schumacher, M.; Baumann, P. K.; Seidel, T., AVD and ALD as Two Complementary Technology Solutions for Next Generation Dielectric and Conductive Thin-Film Processing. *Chemical Vapor Deposition* **2006,** 12, (2-3), 99-108.
27. Rodriguez, B. J.; Callahan, C.; Kalinin, S. V.; Proksch, R., Dual-frequency resonance-tracking atomic force microscopy. *Nanotechnology* **2007,** 18, (47), 475504.
28. Ihlefeld, J. F.; Tian, W.; Liu, Z. K.; Doolittle, W. A.; Bernhagen, M.; Reiche, P.; Uecker, R.; Ramesh, R.; Schlom, D. G. In *Adsorption-controlled growth of $BiFeO_3$ by MBE and integration with wide band gap semiconductors*, Applications of Ferroelectrics, 2008. ISAF 2008. 17th IEEE International Symposium on the, 23-28 Feb. 2008, 2008; 2008; pp 1-2.
29. Keeney, L.; Kulkarni, S.; Deepak, N.; Schmidt, M.; Petkov, N.; Zhang, P. F.; Cavill, S.; Roy, S.; Pemble, M. E.; Whatmore, R. W., Room temperature ferroelectric and magnetic investigations and detailed phase analysis of Aurivillius phase $Bi_5Ti_3Fe_{0.7}Co_{0.3}O_{15}$ thin films. *Journal of Applied Physics* **2012,** 112, (5), -.
30. Ramesh, R., Materials science: Emerging routes to multiferroics. *Nature* **2009,** 461, (7268), 1218-1219.
31. Ricci, D.; Braga, P., Recognizing and Avoiding Artifacts in AFM Imaging. In *Atomic Force Microscopy*, Braga, P.; Ricci, D., Eds. Humana Press: 2004; Vol. 242, pp 25-37.
32. Zhang, P. F.; Deepak, N.; Keeney, L.; Pemble, M. E.; Whatmore, R. W., The structural and piezoresponse properties of c-axis-oriented Aurivillius phase $Bi_5Ti_3FeO_{15}$ thin films deposited by atomic vapor deposition. *Applied Physics Letters* **2012,** 101, (11), -.
33. Schlom, D. G.; Haeni, J. H.; Lettieri, J.; Theis, C. D.; Tian, W.; Jiang, J. C.; Pan, X. Q., Oxide nano-engineering using MBE. *Materials Science and Engineering: B* **2001,** 87, (3), 282-291.
34. Jesse, S.; Baddorf, A. P.; Kalinin, S. V., Switching spectroscopy piezoresponse force microscopy of ferroelectric materials. *Applied Physics Letters* **2006,** 88, (6), 062908-3.
35. Shelke, V.; Mazumdar, D.; Srinivasan, G.; Kumar, A.; Jesse, S.; Kalinin, S.; Baddorf, A.; Gupta, A., Reduced Coercive Field in $BiFeO_3$ Thin Films Through Domain Engineering. *Advanced Materials* **2011,** 23, (5), 669-672.
36. Jang, H. W.; Baek, S. H.; Ortiz, D.; Folkman, C. M.; Eom, C. B.; Chu, Y. H.; Shafer, P.; Ramesh, R.; Vaithyanathan, V.; Schlom, D. G., Epitaxial (001) $BiFeO_3$ membranes with substantially reduced fatigue and leakage. *Applied Physics Letters* **2008,** 92, (6), -.
37. Kay, H. F.; Dunn, J. W., Thickness dependence of the nucleation field of triglycine sulphate. *Philosophical Magazine* **1962,** 7, (84), 2027-2034.
38. Lichtensteiger, C.; Zubko, P.; Stengel, M.; Aguado-Puente, P.; Triscone, J.-M.; Ghosez, P.; Junquera, J., Ferroelectricity in Ultrathin-Film Capacitors. In *Oxide Ultrathin Films*, Wiley-VCH Verlag GmbH & Co. KGaA: 2011; pp 265-230.
39. Wang, Y.; Niranjan, M. K.; Janicka, K.; Velev, J. P.; Zhuravlev, M. Y.; Jaswal, S. S.; Tsymbal, E. Y., Ferroelectric dead layer driven by a polar interface. *Physical Review B* **2010,** 82, (9), 094114.
40. Dawber, M.; Chandra, P.; Littlewood, P. B.; Scott, J. F., Depolarization corrections to the coercive field in thin-film ferroelectrics. *Journal of Physics: Condensed Matter* **2003,** 15, (24), L393.
41. Soergel, E., Piezoresponse force microscopy (PFM). *Journal of Physics D: Applied Physics* **2011,** 44, (46), 464003.
42. Zhao, J. L.; Lu, H. X.; Sun, J. R.; Shen, B. G., Thickness dependence of piezoelectric property of ultrathin $BiFeO_3$ films. *Physica B: Condensed Matter* **2012,** 407, (12), 2258-2261.
43. Scott, J. F.; Paz de Araujo, C. A., Ferroelectric Memories. *Science* **1989,** 246, (4936), 1400-1405.

TABLE OF CONTENTS GRAPHIC

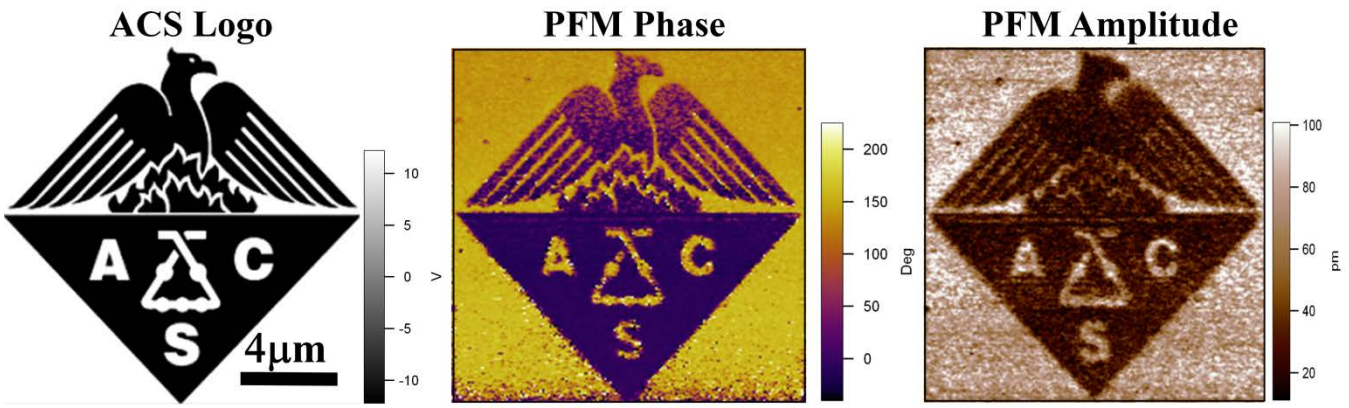


**Information written in the form of ACS logo on ferroelectric film with PFM**

# Bismuth Self-Limiting Growth of ultra-thin $BiFeO_3$ Films

*Nitin Deepak[†,‡,*], Patrick Carolan[†], Lynette Keeney[†], Panfeng F. Zhang[†], Martyn E. Pemble[†,‡] and Roger W. Whatmore[†,‡,§,*]*

[†]Tyndall National Institute, University College Cork, 'Lee Maltings', Dyke Parade, Cork, Ireland

[‡]Department of Chemistry, University College Cork, Dyke Parade, Cork, Ireland

[§] Department of Materials, Faculty of Engineering, Imperial College London, London, SW7 2AZ, UK

SUPPORTING INFORMATION

"This material is available free of charge via the Internet at http://pubs.acs.org."

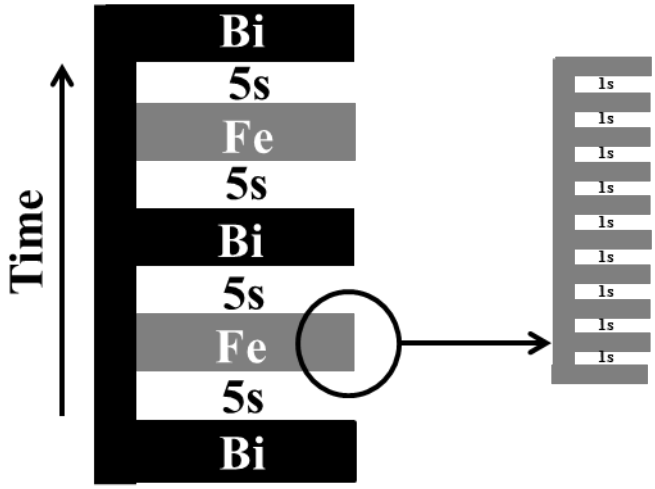


**Figure S1** The precursor injection sequence (alternating injection mode) used for the growth of $BiFeO_3$ thin films. The bismuth and iron precursors are injected in an alternating fashion, with a time difference of 5s (or 10s, or 15s) between each set of pulses. The zoomed-in image shows the structure of a single Fe pulse set which is made up of individual Fe pluses with 1Hz frequency.

**Table S1.** Bismuth and Iron precursor pulse width and pulse number for the first two sets of experiments.

| Bi/Fe Ratio | Bi Opening Time (ms) | Bi Pulse Number | Fe Opening Time (ms) | Fe Pulse Number | Growth Rate (nm/cycle) |
|---|---|---|---|---|---|
| **Iron Change** | | | | | |
| **3.32** | 4 | 10 | 2.5 | 5 | 0.20 |
| **2.95** | 4 | 10 | 3 | 5 | 0.30 |
| **2.30** | 4 | 10 | 4 | 5 | 0.39 |
| **2.09** | 4 | 10 | 4.5 | 5 | 0.41 |
| **1.94** | 4 | 10 | 5 | 5 | 0.48 |
| **Bi Change** | | | | | |
| **2.60** | 6 | 10 | 5 | 5 | 0.47 |
| **1.99** | 5 | 10 | 5 | 5 | 0.49 |
| **1.81** | 4.5 | 10 | 5 | 5 | 0.50 |
| **1.77** | 3.5 | 10 | 5 | 5 | 0.51 |
| **1.33** | 3 | 10 | 5 | 5 | 0.51 |

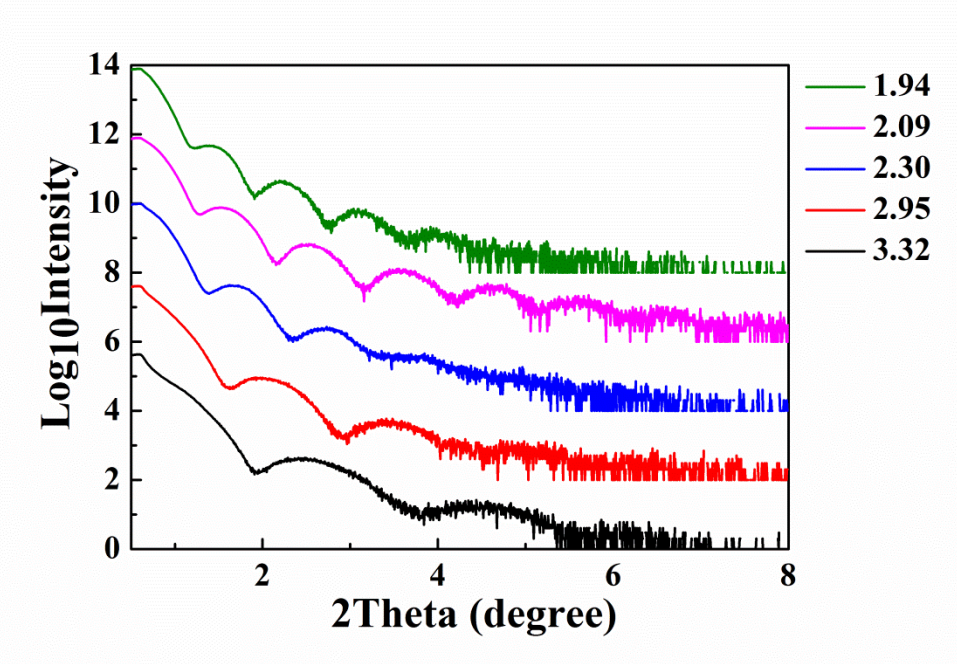


**Figure S2** X-ray reflection (XRR) plots for thin films prepared by keeping the bismuth precursor flow constant and varying the iron precursor flow.

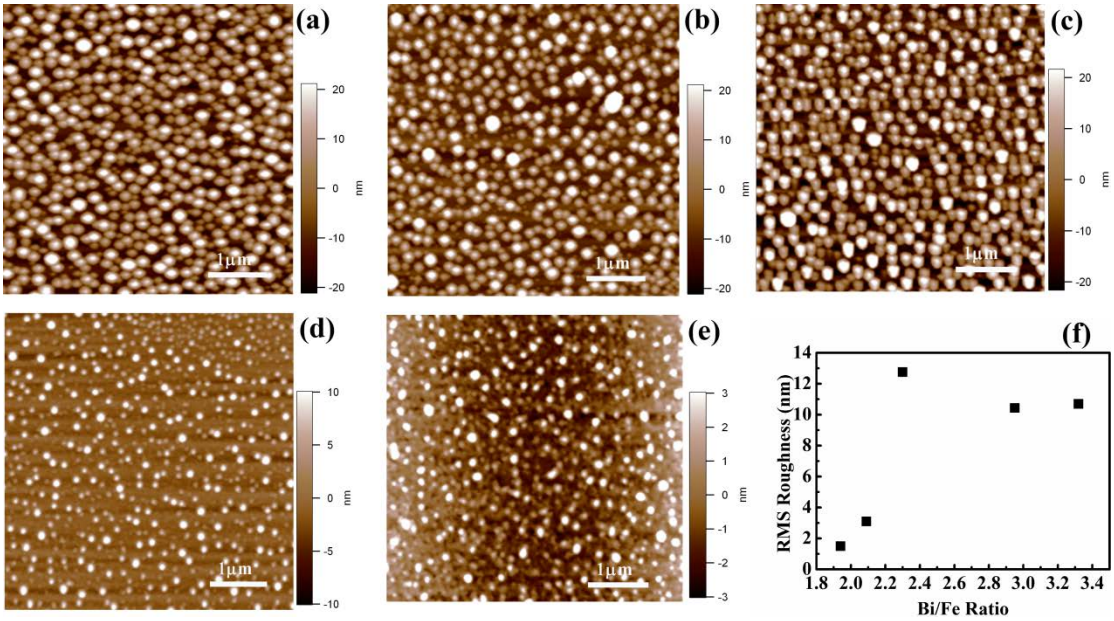


**Figure S3** AFM images for thin films prepared by keeping the bismuth precursor flow constant and varying the iron precursor flow with Bi/Fe ratios of **(a)** 3.32, **(b)** 2.95, **(c)** 2.30**, (d)** 2.09 and **(e)** 1.94. **(f)** Illustrates the variation of RMS roughness with Bi/Fe ratio.

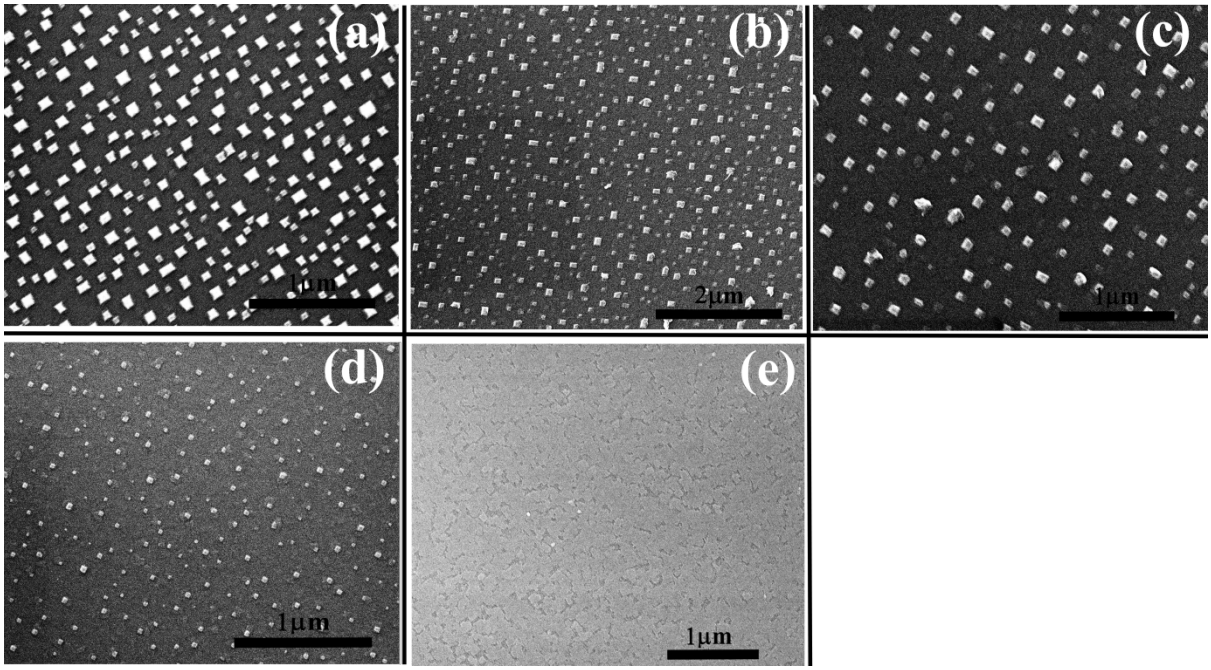


**Figure S4** The SEM images for thin films prepared by keeping the bismuth precursor flow constant and varying the iron precursor flow. The images at Bi/Fe ratios of **(a)** 3.32, **(b)** 2.95, **(c)** 2.30**, (d)** 2.09, and **(e)** 1.94.

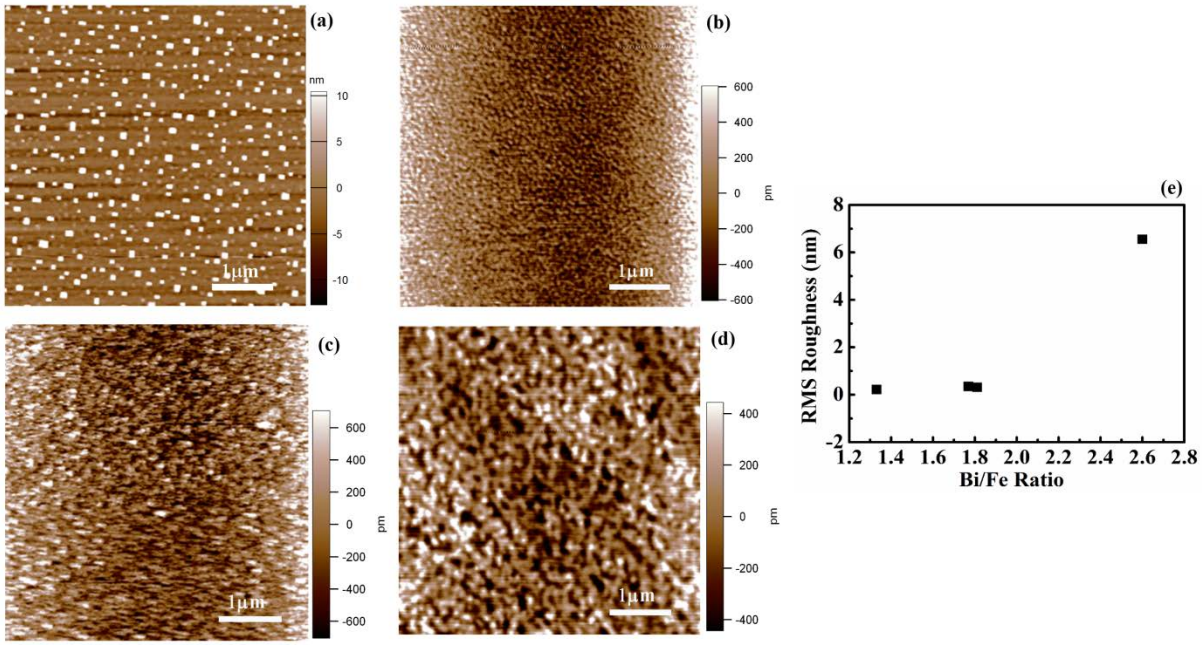


**Figure S5** AFM images for thin films prepared by keeping the iron precursor flow constant and varying the bismuth precursor flow with Bi/Fe ratios of **(a)** 2.60, **(b)** 1.81, **(c)** 1.77 and **(d)** 1.33. **(e)** Illustrates the variation of RMS roughness with Bi/Fe ratio.

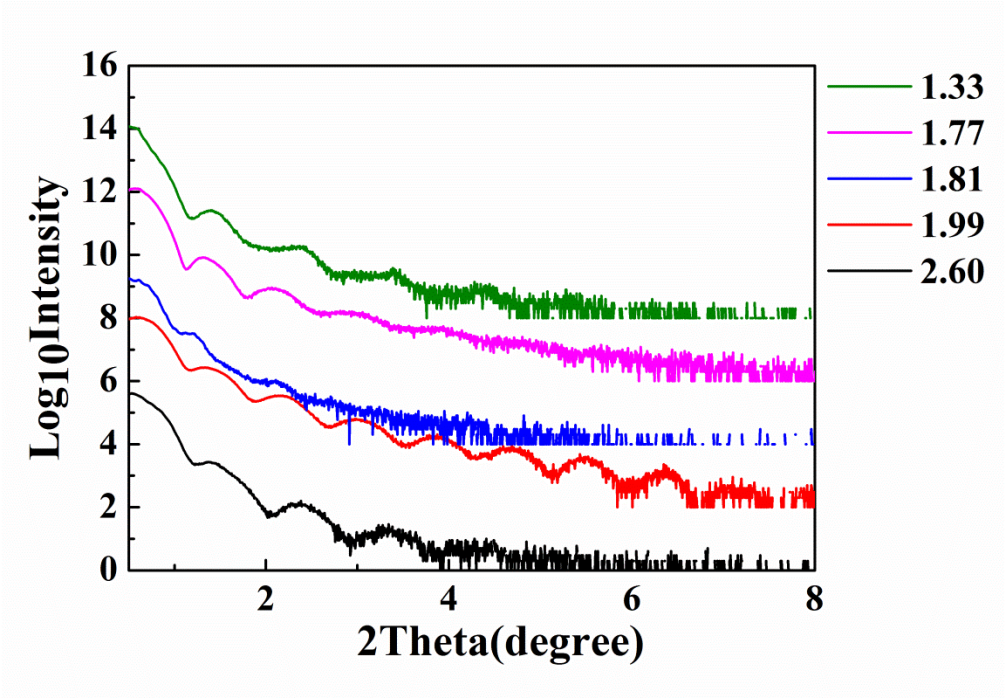


**Figure S6** X-ray reflection (XRR) plots for thin films prepared by keeping the iron precursor flow constant and varying the bismuth precursor flow.

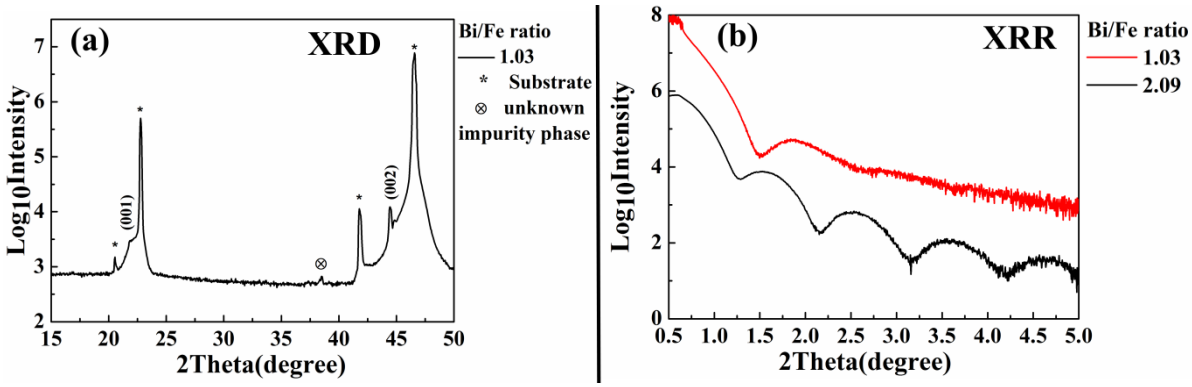


**Figure S7 (a)** XRD plot for films grown at Bi/Fe ratio of 1.03 and **(b)** XRR plot for films grown at a Bi/Fe ratios 1.03 and 2.09.

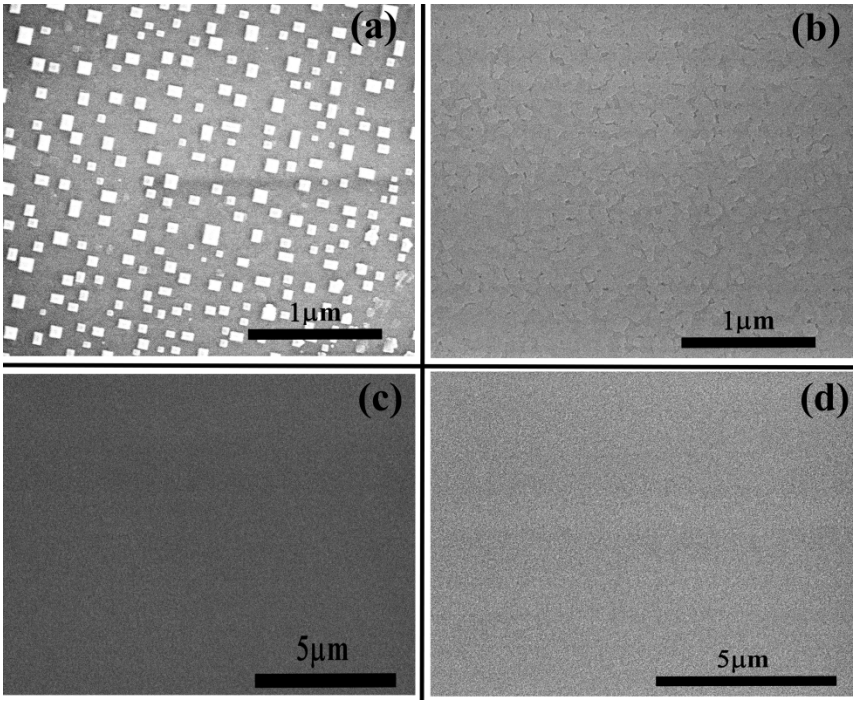


**Figure S8** The SEM images for thin films prepared by keeping the iron precursor flow constant and varying the bismuth precursor flow. The images at Bi/Fe ratios of **(a)** 2.60, **(b)** 1.81, **(c)** 1.77, and **(d)** 1.33.

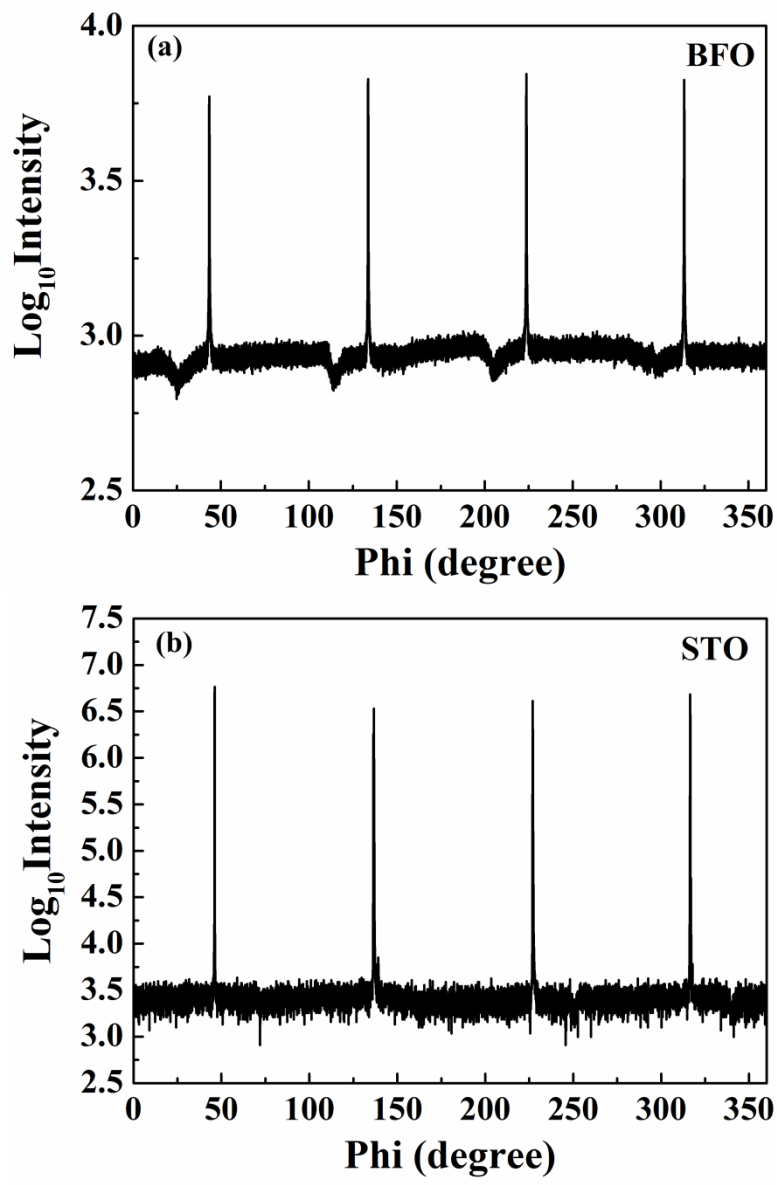


**Figure S9** The in-plane phi scan for (a) the (101) BFO peak and (b) the (202) STO peak. The presence of four peaks at 90° distances confirms the pseudo cubic symmetry of the BFO film on STO substrates.

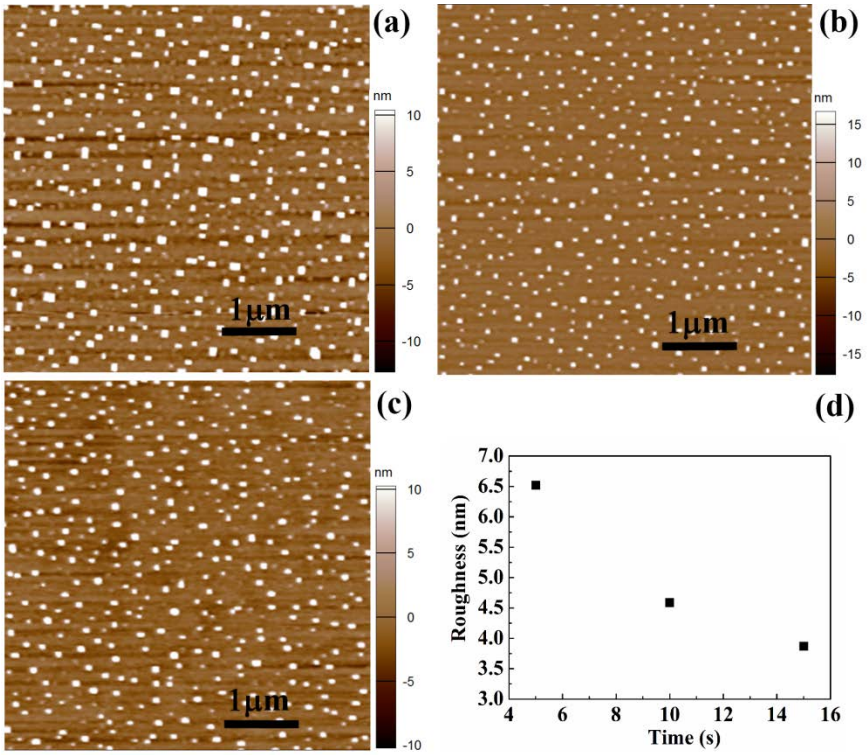


**Figure S10** AFM images for thin films prepared by keeping the bismuth and iron precursor flow constant and varying the time difference between each set of pulses: **(a)** 5s, **(b)** 10s and **(c)** 15s. **(d)** Illustrates the variation of RMS roughness at different times.

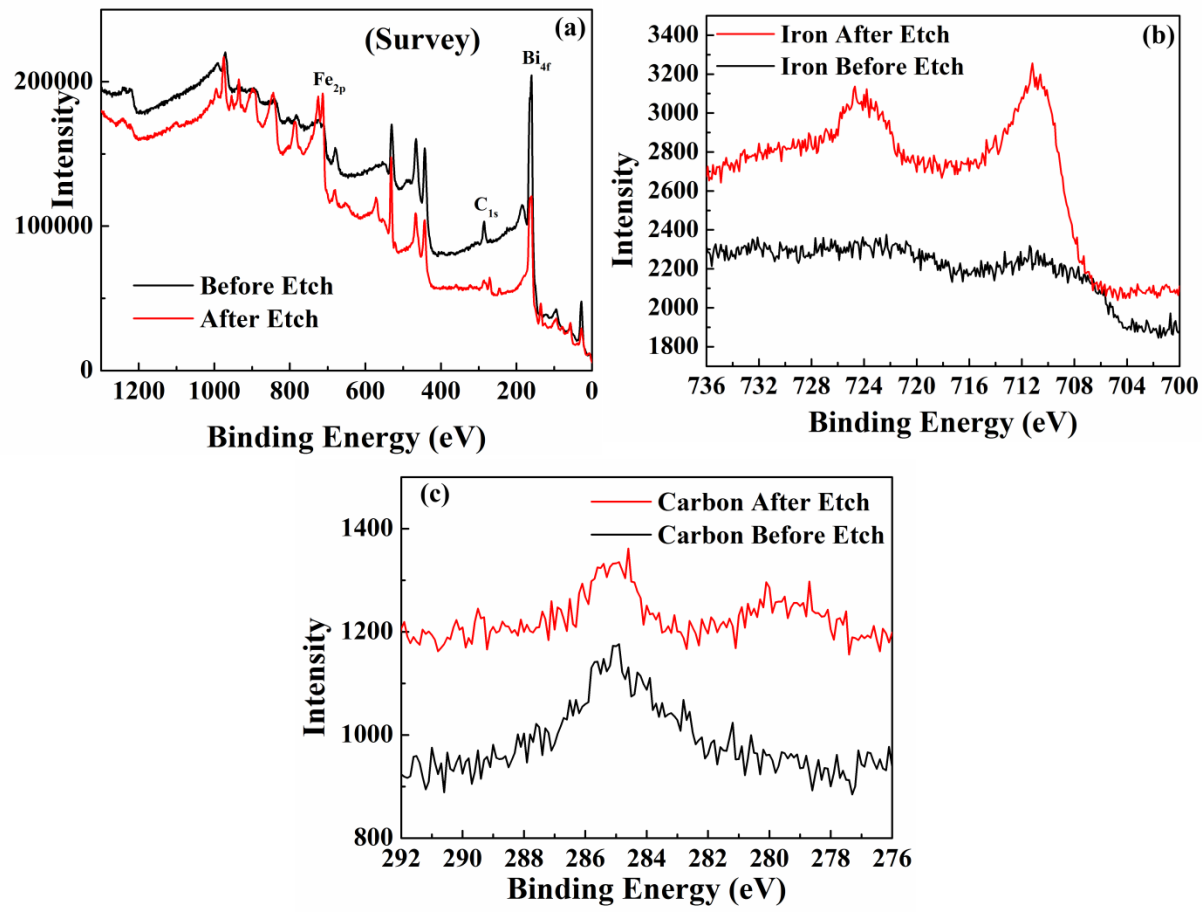

**Figure S11** XPS analysis of a sample with a Bi/Fe ratio of 1.77 from the second set of experiments before and after Ar ion etch cleaning. The Ar ion cleaning helps in achieving better signal to noise ratio by cleaning the surface carbon from the films. XPS **(a)** survey scan, **(b)** Fe $2p_{3/2}$ (711.04 eV) and $2p_{1/2}$ (724.05 eV), and **(c)** C1s peak (285 eV). The C1s peak was used for calibrating the XPS data. The position of the Fe 2p edge confirms the presence of $Fe^{3+}$ and there was no evidence of $Fe^{2+}$ in the films within the detection limit of XPS.

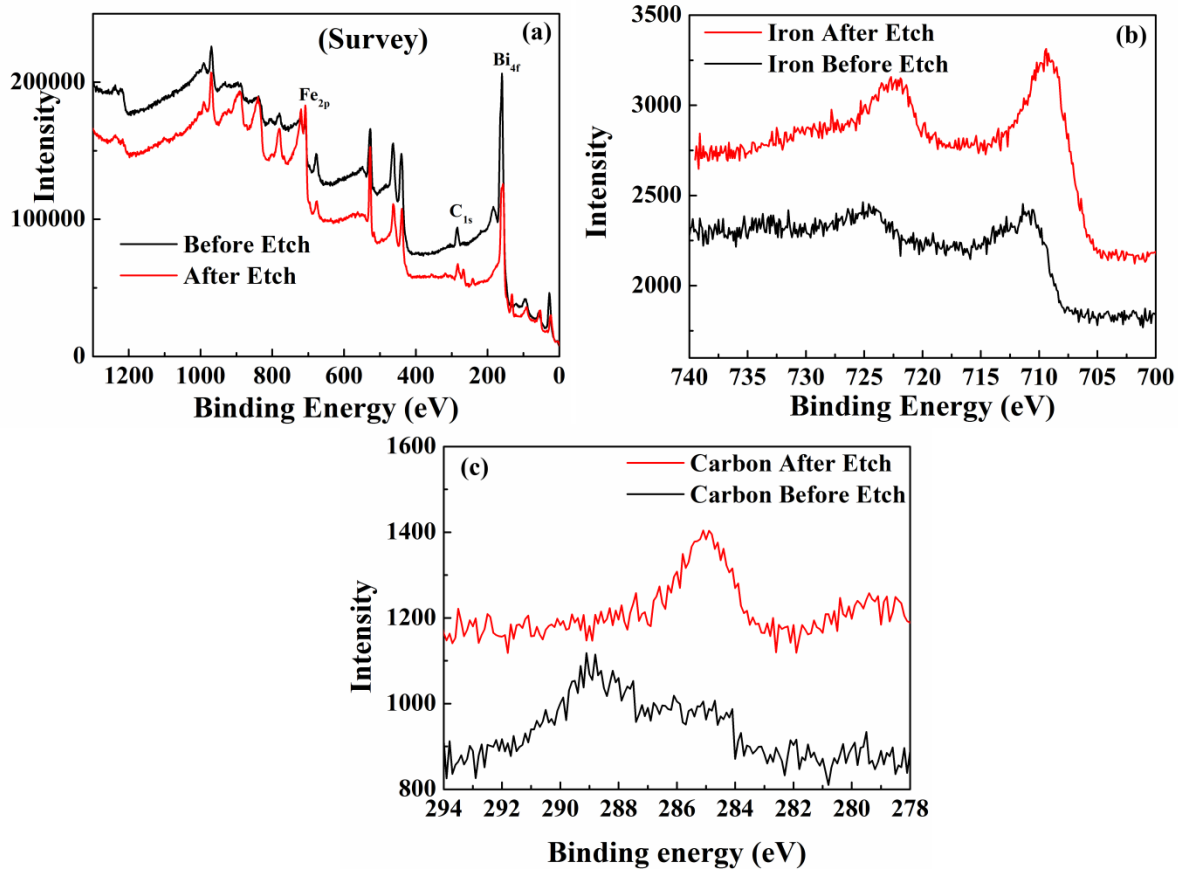


**Figure S12** XPS analysis of a sample with a Bi/Fe ratio of 1.33 from the second set of experiments before and after Ar ion etch cleaning. The Ar ion cleaning helps in achieving better signal to noise ratio by cleaning the surface carbon from the films. XPS **(a)** survey scan, **(b)** Fe $2p_{3/2}$ and $2p_{1/2}$, and **(c)** C1s peak (285 eV). The C1s peak was used for calibrating the XPS data. The Fe 2p edge shows considerable difference between peak positions before and after Ar ion cleaning. The position of Fe $2p_{3/2}$ shifts from 711.15 eV to 709.5 eV and Fe $2p_{1/2}$ changes from 724.9 eV to 722.56 eV after Ar ion cleaning. This shift is due to the creation of oxygen vacancies due to cleaning. The presence at of an extra peak at 289 eV near the C1s peak at 285 eV shows the presence of other forms of carbon which diminishes after Ar ion cleaning.

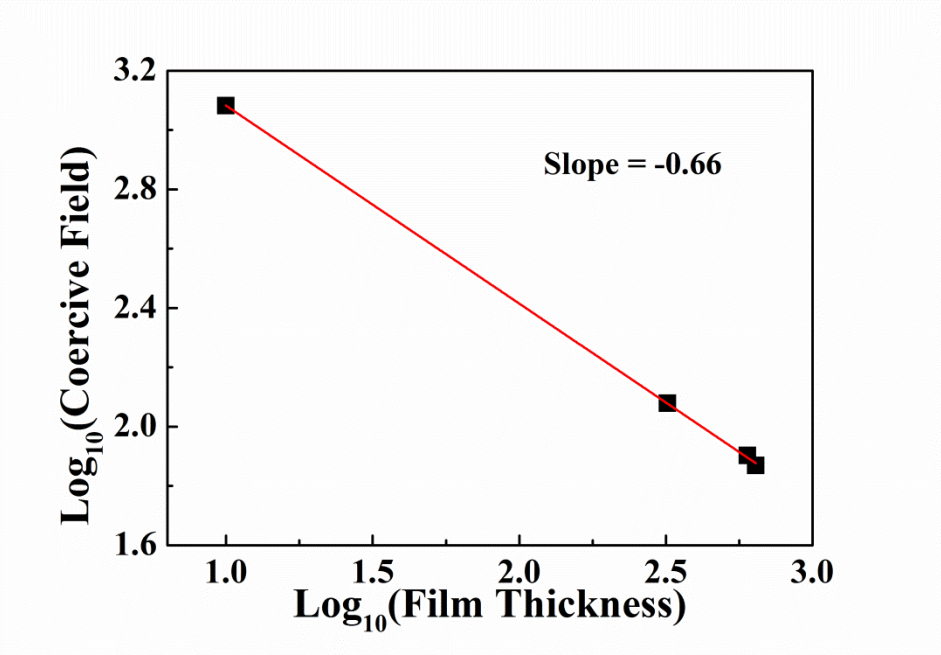


**Figure S13** Extrapolation of coercive field for 10nm BFO films from the Kay-Dunn scaling law $E_C \alpha t^{-2/3}$ (where t is film thickness), using values from literature[1-3].

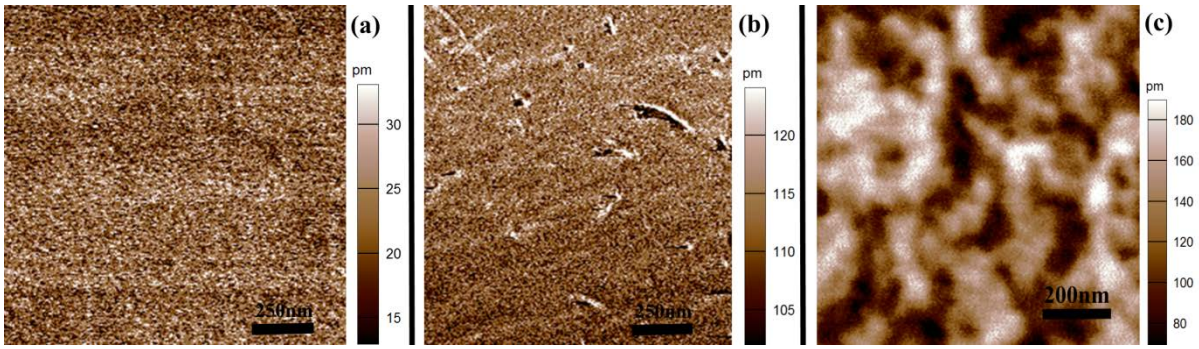


**Figure S14** The PFM amplitude image for **(a)** silicon, **(b)** α-quartz, and **(c)** BFO used to calculate the $d_{33}$ value for BFO thin film.

## References

1. Kay, H. F.; Dunn, J. W., Thickness dependence of the nucleation field of triglycine sulphate. *Philosophical Magazine* **1962,** 7, (84), 2027-2034.
2. Shelke, V.; Mazumdar, D.; Srinivasan, G.; Kumar, A.; Jesse, S.; Kalinin, S.; Baddorf, A.; Gupta, A., Reduced Coercive Field in $BiFeO_3$ Thin Films Through Domain Engineering. *Advanced Materials* **2011,** 23, (5), 669-672.
3. Jang, H. W.; Baek, S. H.; Ortiz, D.; Folkman, C. M.; Eom, C. B.; Chu, Y. H.; Shafer, P.; Ramesh, R.; Vaithyanathan, V.; Schlom, D. G., Epitaxial (001) $BiFeO_3$ membranes with substantially reduced fatigue and leakage. *Applied Physics Letters* **2008,** 92, (6), -.